

Neural Spectral Marked Point Processes

Shixiang Zhu[†], Haoyun Wang[†], Xiuyuan Cheng^{*}, Yao Xie[†]

June 22, 2021

Abstract

Self- and mutually-exciting point processes are popular models in machine learning and statistics for dependent discrete event data. To date, most existing models assume stationary kernels (including the classical Hawkes processes) and simple parametric models. Modern applications with complex event data require more general point process models that can incorporate contextual information of the events, called marks, besides the temporal and location information. Moreover, such applications often require non-stationary models to capture more complex spatio-temporal dependence. To tackle these challenges, a key question is to devise a versatile influence kernel in the point process model. In this paper, we introduce a novel and general neural network-based non-stationary influence kernel with high expressiveness for handling complex discrete events data while providing theoretical performance guarantees. We demonstrate the superior performance of our proposed method compared with the state-of-the-art on synthetic and real data.

1 Introduction

Event sequence data are ubiquitous in our daily life, ranging from traffic incidents, 911 calls, social media posts, and earthquake catalogs. Such data consist of a sequence of events indicating when and where each event occurred, with additional descriptive information (called *marks*) about the event (such as category, volume, or free-text). The distribution of events is of scientific and practical interest, both for prediction purposes and for inferring events' underlying generative mechanism.

A popular framework for modeling events is point processes [3], which can be continuous over time and the space of marks. An important aspect of this model is capturing the event's triggering effect on its subsequent events. Since the distribution of point processes is completely specified by the conditional intensity function (the occurrence rate of events conditioning on the history), such triggering effect has been captured by an influence kernel function embedded in the conditional intensity. In statistical literature, the kernel function usually assumes a parametric form. For

^{*}Department of Mathematics, Duke University.

[†]H. Milton Stewart School of Industrial and Systems Engineering, Georgia Institute of Technology. Email: yao.xie@isye.gatech.edu.

example, the original work by Hawkes [6] considers an exponential decaying influence function over time, and the seminal work [15] introduces epidemic-type aftershock sequence (ETAS) model, which considers an influence function that exponentially decays over space and time. With the increasing complexity of modern applications, there has been much recent effort in developing recurrent neural network (RNN)-based point processes, leveraging the rich representation power of RNNs [4, 10, 24].

However, there are several limitations of existing RNN-based models. First, such models typically do not consider the kernel function [4, 8, 10, 20, 23, 24]; thus, the RNN approach does not enjoy the interpretability of the kernel function based models. Second, the popular RNN models such as Long Short-Term Memory (LSTM) [7] still implicitly discounts the influence of events over (due to their recursive structure) [21, 30]. Such assumptions may not hold in many real-world applications. Take the earthquake catalog as an example, which is a typical type of discrete event data; most aftershocks occur along the fault plane or other faults within the volume affected by the mainshock’s strain [27]. This means that different regions may be correlated to their surrounding area differently according to their geological structure, which creates a complex non-stationary spatial profile that we would like to capture through the model. Third, a majority of the existing works mainly focus on one-dimensional temporal point processes. Although there are works on marked point processes [4, 10, 17], they are primarily based on simplifying assumptions that the marks are conditionally independent of the event’s time and location, which is equivalent to assuming the kernel is separable; these assumptions may fail to capture some complex non-stationary, time- and location-dependent triggering effects for various types of events.

Contribution. In this paper, we present a novel general non-stationary point process model based on neural networks, referred to as the neural spectral marked point process (NSMPP). The key component is a new powerful representation of the kernel function using neural networks, which enables us to go beyond stationarity (and thus go beyond Hawkes processes) and has the capacity to model high-dimensional marks. The premise of the model design is that the conditional intensity function uniquely specifies the distribution of the point process, and the most important component in the intensity function is the influence kernel. In summary, the novelty of our approach includes the following:

- The kernel function is represented by a spectral decomposition of the influence kernel with a finite-rank truncation in practice. Such a kernel representation will enable us to capture the most general non-stationary process as well as high-dimensional marks. The model also allows the distribution of marks to depend on time, which is drastically different from the separable kernels considered in the existing literature [17].
- The spectral decomposition of asymmetric influence kernel consists of a sum of the product of feature maps, which can be parameterized by neural networks. This enable us to harvest the powerful expressiveness and scalability to high-dimensional input of neural networks for complicated tasks involving discrete events data.
- We establish theoretical guarantees of the maximum likelihood estimate for the true kernel

function based on functional variational analysis and finite-dimensional asymptotic analysis, which shed light on theoretical understanding of neural network-based kernel functions.

- Using synthetic and real data (seismic and police data), we demonstrate the superior performance of our proposed method in complex situations; the performance gain is particularly outstanding for cases involving non-stationary point processes.

Related work. Seminal works in point processes modeling [14, 15] assume parametric forms of the intensity functions. Such methods enjoy good interpretability and are efficient to estimate. However, classical parametric models are not expressive enough to capture the events' dynamics in modern applications.

Recent research interests aim to improve the expressive power of point process models, where a recurrent neural networks (RNNs)-based structure is introduced to represent the conditional intensity function [4, 10, 24]. However, most of these works either explicitly or implicitly specify the inter-event dependence in a limited form with restrained representative power. For example, [4] expresses the influence of two consecutive events in a form of $\exp\{w(t_{i+1} - t_i)\}$, which is an exponential function with respect to the length of the time interval $t_{i+1} - t_i$ with weights w ; [10] enhances the expressiveness of the model and represents the entire history using the hidden state of an LSTM, which still implicitly assumes the influence of the history decays over time due to the recurrent structure of LSTM.

Another line of research uses neural networks to directly model dependence of sequential events without specifying the conditional intensity function explicitly [8, 23]. Some studies consider non-stationary influence kernel using neural networks in spatio-temporal point processes [26, 27]. Recent work [16] also uses a neural network to parameterize the hazard function, the derivative of which gives the conditional intensity function. However, the above approaches either capture the temporal dependence or assume the temporal and mark dependence are separable rather than jointly accounting for marked-temporal dependence.

Recently, attention models have become popular in computer vision and sequential data modeling [2, 9, 21]. This motivates works including [25, 29–31] to model the conditional intensity of point processes using the attention mechanism and characterize the inter-event dependence by a score function. The attention mechanism has proven to be more flexible in capturing long-range dependence regardless of how far apart two events are separated and greatly enhances the performance in practice. However, the main limitation of [25, 31] is that they rely on a conventional score function – dot-product between linear mappings of events, which is still limited in representing non-linear dependence between events for some applications. [28–30] used a more flexible and general Fourier kernel as a substitution for the dot-product score; however, the expressive power of the proposed Fourier kernel is still limited, and the spectrum of the Fourier basis is represented by a generative neural network, which is difficult to learn in some cases [1].

There are also works [18, 19] studying non-stationary kernels combined with Gaussian processes, assuming specific structures of the kernels in the Fourier domain. Such kernels are more restricted than ours since the nature of Gaussian processes requires that the kernel is positive semidefinite.

2 Method

2.1 Background: Marked temporal point process

Marked temporal point processes (MTPPs) [17] consist of a sequence of events over time. Each event is associated with a (possibly multi-dimensional) *mark* that contains detailed information of the event, such as location, nodal information (if the observations are over networks, such as sensor or social networks) categorical data, and contextual information (such as token, image, and text descriptions). Let $T > 0$ be a fixed time-horizon, and $\mathcal{M} \subseteq \mathbb{R}^d$ be the space of marks. We denote the space of observation as $\mathcal{X} = [0, T) \times \mathcal{M}$ and a data point in the discrete event sequence as

$$x = (t, m), \quad t \in [0, T), \quad m \in \mathcal{M}, \quad (1)$$

where t is the event time and m represents the mark. Let N_t be the number of events up to time $t < T$ (which is random), and $\mathcal{H}_t := \{x_1, x_2, \dots, x_{N_t}\}$ denote historical events. Let \mathbb{N} be the counting measure on \mathcal{X} , i.e., for any measurable $S \subseteq \mathcal{X}$, $\mathbb{N}(S) = |\mathcal{H}_T \cap S|$. For any function $f : \mathcal{X} \rightarrow \mathbb{R}$, the integral with respect to the counting measure is defined as

$$\int_S f(x) d\mathbb{N}(x) = \sum_{x_i \in \mathcal{H}_T \cap S} f(x_i).$$

The events' distribution in MTPPs can be characterized via the *conditional intensity function* $\lambda(x)$, which is defined to be the conditional probability of observing an event in the marked temporal space \mathcal{X} given the events' history $\mathcal{H}_{t(x)}$, that is,

$$\mathbb{E}(d\mathbb{N}(x) | \mathcal{H}_{t(x)}) = \lambda(x) dx.$$

Above, $t(x)$ extracts the occurrence time of event x , and we omit the dependence on $\mathcal{H}_{t(x)}$ in the notation of $\lambda(x)$ for simplicity.

As self- and mutual-exciting point processes, Hawkes processes [6] have been widely used to capture the mutual excitation dynamics among temporal events. The model assumes that influences from past events are linearly additive towards the current event. The conditional intensity function for a self-exciting point process takes the form of $\lambda[k](x) = \mu + \sum_{x' \in \mathcal{H}_{t(x)}} k(x', x)$, where $\mu > 0$ stands for the background intensity, and the so-called ‘‘influence kernel’’ $k : \mathcal{X} \times \mathcal{X} \rightarrow \mathbb{R}$ is crucial in capturing the influence of past events on the likelihood of event occurrence at the current time. Here we use the notation $[k]$ to stress the dependence of the conditional intensity function on the kernel function $k(x', x)$. Written in the form of the integral over counting measure, we have that

$$\lambda[k](x) = \mu + \int_{x' \in \mathcal{X}_{t(x)}} k(x', x) d\mathbb{N}(x'), \quad (2)$$

where \mathcal{X}_t is the subset of \mathcal{X} with the first component smaller than t .

The most commonly made assumption in the literature is that the process is stationary, where

the influence of the past events is shift-invariant, such that $k(x', x) = f(x - x')$ for a influence function $f : \mathbb{R}^d \rightarrow \mathbb{R}^+$; a common influence function in one-dimensional cases is $f(t) = \alpha \exp\{-\beta t\}$, where β controls the decay rate and $\alpha > 0$ controls the magnitude of the influence of an event. The current work aims at going beyond stationary point processes, which enables us to better capture the heterogeneity in the events' influence across the spatial-temporal space, which naturally arises in many applications.

2.2 Neural spectral representation for influence kernel

We propose to represent more general non-stationary influence kernels in the conditional intensity function $\lambda(x)$ specified in (2).

Kernel representation. The main idea of the proposed model is to represent the influence kernel k using a general finite-rank decomposition

$$k(x', x) = \sum_{r=1}^R \nu_r \psi_r(x') \phi_r(x), \quad \nu_r \geq 0, \quad (3)$$

where

$$\psi_r : \mathcal{X} \rightarrow \mathbb{R}, \quad \phi_r : \mathcal{X} \rightarrow \mathbb{R}, \quad r = 1, \dots, R,$$

are two sets of *feature functions* in some smooth functional space $\mathcal{F} \subset C^0(\mathcal{X})$, and ν_r is the corresponding weight - or “spectrum”. This representation is motivated by the spectral decomposition of a general kernel function. While functional spectral decomposition is usually infinitely dimensional, for practical considerations, we truncate the “spectrum” and only consider a finite

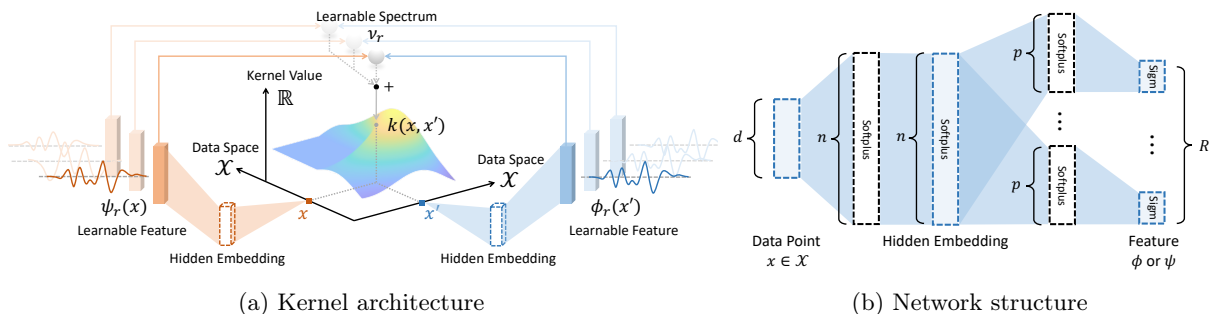


Figure 1: (a) The architecture of the proposed non-stationary neural spectral kernel. A hidden embedding will first summarize the data point; then, the embedding will be mapped to different features via multi-branch neural networks. The kernel value is calculated by summing up the products between two sets of learned features, $\{\psi_r\}$ and $\{\phi_r\}$, weighted by the spectrum $\{\nu_r\}$. The spectrum, feature functions, and hidden embeddings are jointly learned from data. (b) The structure of the multi-branch neural network. There are two shared layers with n nodes per layer that generate the hidden embedding; d denotes the dimension of the input data point; p denotes the dimension of the middle layer that generates the feature. Further specifications of neural networks will be provided in the experiments in Section 4.

rank representation. Note that while we view (3) as similar to a spectral decomposition, it can be better understood as feature maps in kernel representation, and, particularly, we do not need the feature functions ψ_r and ϕ_r to be orthogonal.

The decomposition (3) represents the kernel function using three parts: two sets of (normalized) feature functions and the energy spectrum—the spectrum ν_r plays the role of weights to combine the feature maps. In the learning process, we can train the feature functions (typically neural networks) and the weights separately; since learning the normalized feature maps tend to be more numerically stable. The proposed form of kernel is not necessarily positive semi-definite, and even not symmetric. Note that the spectral representation can allow for a completely general kernel that can be used for non-stationary processes (since our influence function does not impose a shift-invariant structure). Moreover, the spectral representation allows us to go beyond monotone decay or parametric form as commonly assumed in the prior literature.

Neural network feature function. As one of the most salient features of our method, feature functions $\{\phi_r, \psi_r\}$ are represented using neural networks, leveraging their known universal approximation power. First, the input data point $x \in \mathcal{X}$ will be projected to a hidden embedding space via a multi-layer shared network, aiming to extract key information of the input data. Here we have adopted Softplus non-linear activation in this feature extraction sub-network, while other options may be possible. Next, the hidden embedding will be mapped to the different features $\{\phi_r(x)\}$ through R branched sub-networks. To ensure the output feature is constrained in a bounded space, we choose the scaled sigmoidal function as the activation of the output layer, i.e., $f(x) = s/(1 + \exp(-x))$, where s is a constant to enable rescaling of the output to a proper range (in our setting, we set s to be 100). The overall architecture of our kernel formulation and the structure of the multi-branch neural network are summarized in Figure 1 (a) and (b), respectively. Further specifications of neural networks will be provided in the experiments in Section 4.

2.3 Maximum likelihood model recovery

An essential task in learning the neural point process model is to estimate the influence kernel function for the point process. The reason is two-fold: First, the kernel function is the most important component in representing the point process. Second, in practice, the influence kernel offers clear interpretations, such as “how events at a particular time and location will influence future events at a given time and location.” Such interpretation is essential for predicting using event data— one of the main applications for point process models.

To estimate the influence kernel function for point process models, we consider a popular approach through maximum likelihood estimation (MLE). Formally, the optimal kernel can be found by solving the following optimization problem given M sequences of training event sequences over the time horizon $[0, T]$: $\{x_{i,j}\}$, $i = 1, \dots, N_j$, $j = 1, \dots, M$:

$$\max_{k \in \mathcal{K}} \ell[k] := \frac{1}{M} \sum_{j=1}^M \left(\int_{\mathcal{X}} \log \lambda_j[k](x) d\mathbb{N}_j(x) - \int_{\mathcal{X}} \lambda_j[k](x) dx \right), \quad (4)$$

where λ_j and \mathbb{N}_j denote the conditional intensity and counting measure associated with the j -th trajectory, respectively, and $\mathcal{K} \subset C^0(\mathcal{X} \times \mathcal{X})$ represents the family of regular kernel functions induced by the feature function family \mathcal{F} and the finite-rank decomposition (3).

In practice, the kernel function k can be parameterized, for instance, by neural networks. The learning algorithm for model parameter estimation is based on maximum likelihood estimation (MLE), which is presented below. We maximize ℓ using a stochastic gradient as summarized in Algorithm 1. In particular, to calculate the log-likelihood function ℓ in (4), we need to evaluate an integral (the second term), which does not have a closed-form expression. Here we approximate the integral numerically by Monte Carlo integration – drawing a number of samples and take average, which is described in Algorithm 2. Below in Section 3, we will show the theoretical guarantee for the proposed MLE-based kernel function recovery.

Algorithm 1: Stochastic gradient-based learning algorithm

Input: $X = \{\mathbf{x}_j\}_{j=1,\dots,N}$ is the training set with N sequences; η is the number of learning iterations; γ is the learning rate; M is the size of a mini-batch;
Initialization: model parameters $\boldsymbol{\theta}_0$;
 $l \leftarrow 0$;
while $l < \eta$ **do**
 Randomly draw M sequences from X denoted as $\widehat{X}_l = \{\mathbf{x}_j\}_{j=1,\dots,M} \subset X$;
 $\boldsymbol{\theta}_{l+1} \leftarrow \boldsymbol{\theta}_l + \gamma \partial \ell / \partial \boldsymbol{\theta}_l$ given \widehat{X}_l ;
 $l \leftarrow l + 1$;
end

Algorithm 2: Monte Carlo estimation for the integral of conditional intensity in (4)

Input: λ denotes the model that we need to evaluate; $\mathbf{x}_j = \{(t_i, m_i)\}_{i=1}^{N_j}$ is an event sequence, where N_j is the number of events in the sequence; \widetilde{N} is the number of samples uniformly drawn from \mathcal{X} ; Λ is the integral of the conditional intensity over the data space;
 $\Lambda \leftarrow 0$;
for $n = 1, \dots, \widetilde{N}$ **do**
 Draw $x_n := (t_n, m_n) \sim \mathcal{X}$;
 $\mathcal{H}_{t(x_n)} \leftarrow \{(t_i, m_i) \in \mathbf{x}_j : t_i < t_n\}$;
 $\Lambda \leftarrow \Lambda + \lambda_j(x_n)$ given $\mathcal{H}_{t(x_n)}$;
end
 $\Lambda \leftarrow |\mathcal{X}| \Lambda / \widetilde{N}$;

3 Theoretical guarantees of MLE

3.1 Functional kernel identifiability by MLE

In this section, we will establish various theoretical properties of maximum likelihood estimate (MLE) to show that it is an effective way to recover the kernel function. We first consider the MLE as a *functional optimization problem*, since when using neural networks to approximate the kernel function, we are interested in such functional approximation results. We show that the expected log-likelihood reaches its maximum at the true kernel with the second-order derivative bounded away from zero, and thus the *true kernel function is identifiable by solving the MLE problem*.

We study the log-likelihood over the family of kernel functions $\bar{\mathcal{K}}$ which contains \mathcal{K} , the family induced by feature functions in \mathcal{F} and non-negative spectrum $\{\nu_r\}_{r=1}^R$. Note that $\bar{\mathcal{K}}$ may go beyond the finite-rank decomposition in (3). Later throughout the theoretical analysis, we omit the spectrum as they can be absorbed into the feature functions. The details are discussed in Remark 3.2.

Assumption 3.1. (A1) The kernel function family $\bar{\mathcal{K}} \subset C^0(\mathcal{X} \times \mathcal{X})$, and kernel functions in $\bar{\mathcal{K}}$ is uniformly bounded. (A2) There exist c_1, c_2 positive constants, such that for any $k \in \bar{\mathcal{K}}$, $c_1 \leq \lambda_j[k](x) \leq c_2$, $\forall x \in \mathcal{X}$ and $\forall j$.

We have the following lemma, which shows that when the log-likelihood function has a local perturbation around the true kernel function, there is going to be a decrease in the log-likelihood function value in expectation. Note we assume that k^* lies in (or can be well-approximated by) the family of function class \mathcal{K} – thanks to the well-known universal approximation power of neural networks.

Lemma 3.1 (Local perturbation of likelihood function around the true kernel function). *Under Assumption 3.1, for any $\tilde{k} \in \bar{\mathcal{K}}$ and $\delta k = \tilde{k} - k^*$, we have*

$$\ell[k^*] - \ell[\tilde{k}] \geq \frac{1}{M} \left\{ - \sum_{j=1}^M \int_{\mathcal{X}} \delta \lambda_j(x) \left(\frac{d\mathbb{N}_j(x)}{\lambda_j[k^*](x)} - dx \right) + \frac{1}{2c_2^2} \sum_{j=1}^M \int_{\mathcal{X}} (\delta \lambda_j(x))^2 d\mathbb{N}_j(x) \right\}, \quad (5)$$

where

$$\delta \lambda_j(x) := \int_{\mathcal{X}_t(x)} \delta k(x', x) d\mathbb{N}_j(x'). \quad (6)$$

The implication of Lemma 3.1 is the following. Note that in (5), we have nicely decomposed the difference in the likelihood function caused by a small perturbation around the true kernel function, as two terms: the first term in (5) is a martingale integral (since the conditional expectation of $(d\mathbb{N}_j(x)/\lambda_j[k^*](x) - dx)$ is zero, $\forall j$), and the second term is the integral of a quadratic term against the counting measure. The expectation of the first term is zero due to the property of the martingale process. For the second term, per j ,

$$\int_{\mathcal{X}} (\delta \lambda_j(x))^2 d\mathbb{N}_j(x) \approx \int_{\mathcal{X}} (\delta \lambda_j(x))^2 \lambda_j^*(x) dx \geq c_1 \int_{\mathcal{X}} (\delta \lambda_j(x))^2 dx := c_1 \|\delta \lambda_j\|_2^2, \quad (7)$$

and thus perturbation of the intensity function which corresponds to the second (quadratic) term in (5) will be reflected in the decrease of the log-likelihood, which leads to identifiability of the intensity function. Furthermore, we have the identifiability of the kernel itself, as stated in the following theorem.

Theorem 3.2 (Kernel identifiability using maximum likelihood). *Under Assumption 3.1, the true kernel function k^* is locally identifiable in that k^* is a local minimum solution of maximum likelihood (4) in expectation.*

Remark 3.1 (Function identification and neural network parametrization). Theorem 3.2 derives a result which holds for variational perturbation of the kernel function k in the possibly parametric family \mathcal{K} induced by the feature function family \mathcal{F} . When \mathcal{F} is the class of functions that a neural network can represent, the perturbation δk is induced by the change of network parameters. It is common that in neural network models, parameter identification is difficult to search for (e.g., due to the symmetry of permuting hidden neurons); however, the neural network function identification may still hold, e.g., under the mean-field approximation [11]. Thus the kernel function identification results in Theorem 3.2 is important when learning kernel functions by neural networks.

Remark 3.2 (Finite rank kernel representation). When assuming the parameter representation (3), we represent the true kernel as $k^*(x', x) = \sum_{r=1}^R \nu_r \psi_r^*(x') \phi_r^*(x)$. For theoretical analysis purposes, without loss of generality, we can assume $\nu_r = 1$, $r = 1, \dots, R$, since they can be absorbed into the feature functions. Consider a perturbed kernel where the feature functions are $\tilde{\psi}_r = \psi_r + \delta\psi_r$ and $\tilde{\phi}_r = \phi_r + \delta\phi_r$, and remains to satisfy Assumption 3.1. The kernel function variation δk in (6) can then be written as $\delta k(x', x) = \sum_{r=1}^R (\delta\psi_r(x')\phi_r(x) + \psi_r(x')\delta\phi_r(x) + \delta\psi_r(x')\delta\phi_r(x))$. Note that this corresponds to a finite-rank representation of the kernel function corresponding to the architecture of our proposed neural network based kernel functions.

3.2 MLE guarantee under finite dimensional functional representation

We notice that in practice, the kernel function is usually restricted to some function family space for the problem to be well-defined (given a finite number of events). In this section, we study such a set-up, where the target feature function belongs to a certain parametric function class with a finite number of parameters. This includes, for instance, spline functions, functions represented by Fourier basis, and by neural networks – the main interest of this paper. We are particularly interested in neural networks due to its strong expressive power of functional representation.

We start from a general framework of feature function basis representation. Assume that the feature functions of the kernel can be well-approximated by a linear combination of basis functions: $b_i(x) : \mathcal{X} \rightarrow \mathbb{R}$, $i = 1, \dots, S$:

$$\psi_r(x) = \sum_{i=1}^S \alpha_{ri} b_i(x), \quad \phi_r(x) = \sum_{i=1}^S \beta_{ri} b_i(x), \quad r = 1, \dots, R.$$

Then the kernel function in (3) can be written as $k_A(x', x) = b(x')^T A b(x)$, where $b(x) = (b_1(x), \dots, b_S(x))^T$, and the (p, q) -th entry of the matrix A is given by

$$A_{pq} = \sum_{r=1}^R \nu_r \alpha_{rp} \beta_{rq}.$$

Here we assume each matrix A corresponds to a unique model, i.e. for any $A' \neq A$, there exists $x', x \in \mathcal{X}$ with $t(x') < t(x)$, $k_A(x', x) \neq k_{A'}(x', x)$. Under such a parametrization, we can write the intensity function in (2) as

$$\lambda_A(x) := \lambda[k_A](x) = \mu + \int_{\mathcal{X}_{t(x)}} b(x')^T A b(x) d\mathbb{N}(x') = \mu + \langle \eta(x), A \rangle, \quad (8)$$

which is linear in the vectorized A . Here $\langle \cdot, \cdot \rangle$ is the Frobenius inner product of matrices, and $\eta(x) \in \mathbb{R}^{S \times S}$ is conditioned on $\mathcal{H}_{t(x)}$ with the (p, q) -th entry

$$\eta_{pq}(x) = \int_{\mathcal{X}_{t(x)}} b_p(x') b_q(x) d\mathbb{N}(x').$$

Now the influence kernel estimation problem has been reduced to the problem of estimating the S -by- S matrix A . We will estimate the coefficient matrix A by the Maximum Likelihood Estimator (MLE) in the set of low-rank matrices $\mathcal{A} = \{A \in \mathbb{R}^{S \times S} : k_A \in \mathcal{K}\}$ (recall that \mathcal{K} is the family of kernels which admits the finite-rank decomposition as in (3). By saying \mathcal{A} consists of low-rank matrices, we implicitly assume that $R \ll S$). Also we denote the family of kernel functions that can be represented by the chosen basis functions as

$$\mathcal{K}_{\text{finite}} = \{k_A : A \in \mathcal{A}\}.$$

The MLE is defined as

$$\hat{A}_{\text{MLE}} = \arg \max_{A \in \mathcal{A}} \ell_A,$$

where the log-likelihood ℓ_A is the corresponding variant of (4),

$$\ell_A = \frac{1}{M} \left(\sum_{j=1}^M \int_{\mathcal{X}} \log(\mu + \langle \eta_j(x), A \rangle) d\mathbb{N}_j(x) - \sum_{j=1}^M \int_{\mathcal{X}} (\mu + \langle \eta_j(x), A \rangle) dx \right).$$

- With orthonormal bases, the classical theory has that the recovery of A will ensure the recovery of the original kernel function. With a set of over-complete bases, R is less than S (the number of bases function), and then A is a low-rank matrix, for which case we provide a theory for the recovery of A via MLE (Theorem 3.4).
- More generally, the above framework contains other constructions of $b_i(x)$'s. For example, if $b_i(x)$ are random features, then α_{ri} and β_{ri} can be viewed as weights to combine features.

Random feature model can be naturally viewed as a neural network with one hidden layer, that is, $b_i(x) = \sigma(w_i^T x)$ is the activation on the i -th hidden nodes, and $\sum_i \alpha_i b_i(x)$ gives the second layer output function. Here, w_i are weights in the first layer, and linear combination coefficients α_i are weights in the second layer. Thus, the random feature model corresponds to only training the second layer weights, leaving the 1st layer as randomly initialized. In this case, S is the number of hidden neurons, and R can be interpreted as the number of heads in an attention model.

A few consequences. We derive a few necessary basic results based on the model parametrization for presenting the results. Recall that $\eta(x) \in \mathbb{R}^{S \times S}$ depends only on data and basis but not the coefficient matrix A .

- For each trajectory j , the intensity under parameter A at x has partial derivative

$$\frac{\partial \lambda_{A,j}(x)}{\partial A_{pq}} = \eta_{pq,j}(x).$$

- The score function, i.e., the partial gradient of the log-likelihood function with respect to the coefficient matrix A , is given by

$$\frac{\partial \ell_A}{\partial A_{pq}} = \frac{1}{M} \sum_{j=1}^M \int_{\mathcal{X}} \lambda_{A,j}(x)^{-1} \eta_{pq,j}(x) (d\mathbb{N}_j(x) - \lambda_{A,j}(x) dx).$$

- The Hessian matrix of the log-likelihood function is given by

$$\frac{\partial^2 \ell_A}{\partial A_{pq} \partial A_{rs}} = -\frac{1}{M} \sum_{j=1}^M \int_{\mathcal{X}} \lambda_{A,j}^{-2}(x) \eta_{pq,j}(x) \eta_{rs,j}(x) d\mathbb{N}_j(x).$$

Next, we provide some analysis for the MLE with possible model misspecification, as the true kernel k^* may not fall into $\mathcal{K}_{\text{finite}}$.

Theorem 3.3 (Distance between the true kernel and the optimal fit). *Let $\tilde{A} \in \mathcal{A}$ be the one which maximizes the expected log-likelihood function, i.e.*

$$\tilde{A} = \arg \max_{A \in \mathcal{A}} \mathbb{E}(\ell_A). \quad (9)$$

Under Assumption 3.1, let the ℓ_2 -norm of a kernel be

$$\|k\|_2^2 = \int_{\mathcal{X}} \int_{\mathcal{X}_{t(x)}} k(x', x)^2 dx' dx. \quad (10)$$

Then we have

$$\|k^* - k_{\tilde{A}}\|_2^2 \leq \frac{c_2^5 |\mathcal{M}| T + c_2^4}{c_1^4} \exp(2(c_2 - c_1) |\mathcal{M}| T) D(k^*, \mathcal{K}_{\text{finite}})^2,$$

where $D(k^*, \mathcal{K}_{\text{finite}})$ is the ℓ_2 -distance between the true kernel and the set $\mathcal{K}_{\text{finite}}$,

$$D(k^*, \mathcal{K}_{\text{finite}}) = \min_{k \in \mathcal{K}_{\text{finite}}} \|k^* - k\|_2.$$

Remark 3.3. This theorem holds true for any $k^* \in \bar{\mathcal{K}}$ without the rank- R assumption on kernels. In this case, both feature function approximation by basis and low-rank approximation of the kernel contribute to the estimation error associated with model misspecification.

Next, similar to the classic asymptotic normality of the MLE under model misspecification [22], we have the following result for the low-rank MLE.

Theorem 3.4 (Asymptotic normality of low-rank MLE). *Under Assumption 3.1, Assumption A.1, let the singular value decomposition of \tilde{A} be $\tilde{A} = U\Lambda V^T$. Let \tilde{I} be the expected Hessian matrix of the log-likelihood at \tilde{A} ,*

$$\tilde{I} = \mathbb{E} \left(\frac{\partial^2 \ell_A}{\partial \text{vec}(A) \partial \text{vec}(A)^T} \right) \Big|_{A=\tilde{A}} = -\mathbb{E} \left(\int_{\mathcal{X}} \lambda_{\tilde{A}}^{-2} \text{vec}(\eta(x)) \text{vec}(\eta(x))^T d\mathbb{N}(x) \right),$$

where the matrices are vectorized by concatenating their columns, and let \tilde{J} be the covariance matrix of a single trajectory's score function at \tilde{A} ,

$$\tilde{J} = \text{Cov} \left(\frac{\partial \ell_A}{\partial \text{vec}(A)}, \frac{\partial \ell_A}{\partial \text{vec}(A)^T} \right) \Big|_{A=\tilde{A}},$$

$\tilde{G} \in \mathbb{R}^{S \times S}$ be the expected score at \tilde{A} ,

$$\tilde{G} = \mathbb{E} \left(\frac{\ell_A}{\partial A} \right) \Big|_{A=\tilde{A}}.$$

Let $F = (\mathbb{I}_S \otimes U, V \otimes \mathbb{I}_S) \in \mathbb{R}^{S^2 \times 2SR}$ where \otimes is the Kronecker product, \mathbb{I}_S is the identity matrix of size S ,

$$\tilde{C} = (\tilde{A}^\dagger \otimes \tilde{G}) Q_{S,S} + ((\tilde{A}^\dagger \otimes \tilde{G}) Q_{S,S})^T,$$

where \dagger represents pseudo-inverse and $Q_{a,b} \in \mathbb{R}^{ab \times ab}$ is the permutation matrix such that $\text{vec}(P^T) = Q_{a,b} \text{vec}(P)$ for any a -by- b matrix P . If $F^T(\tilde{I} + \tilde{C})F$ shares the same null-space with F , then the low-rank estimator \hat{A}_{MLE} , solved from the constrained maximum likelihood problem, satisfies

$$\sqrt{M}(\text{vec}(\hat{A}_{\text{MLE}}) - \text{vec}(\tilde{A})) \rightarrow \mathcal{N}(0, F(F^T(\tilde{I} + \tilde{C})F)^\dagger F^T \tilde{J} F(F^T(\tilde{I} + \tilde{C})F)^\dagger F),$$

when $M \rightarrow \infty$.

Remark 3.4 (Parameter recovery guarantee). The result shows that the maximum likelihood estimate for the kernel matrix A converges to the optimal fit \tilde{A} , and the matrices $\tilde{I}, \tilde{J}, \tilde{C}$ captures the residual variance; F projects the variance caused by $\tilde{I}, \tilde{J}, \tilde{C}$ onto the tangent space of the low-rank manifold at \tilde{A} . In practice, the variance term can be estimated empirically; \tilde{J} can be

estimated from the empirical covariance matrix of the score function of each trajectory, while the other matrices can be approximated by the properties of the log-likelihood function at \hat{A}_{MLE} . If the true kernel falls into the kernel family $\mathcal{K}_{\text{finite}}$, both \tilde{I}, \tilde{J} will equal to the Fisher Information, \tilde{G}, \tilde{C} will vanish, which greatly simplify the process of estimating the variance. But with the presence of model misspecification, this is generally not the case.

4 Numerical experiments

This section presents experimental results on both synthetic and real data. We first fit our model using the synthetic data sets and visually examine the recovered kernel structure compared to the oracle. We also compare our proposed model with the other three baseline approaches using both synthetic and real data sets. The performance of the synthetic data sets is evaluated by measuring the mean square error of the conditional intensity prediction. Due to a lack of true knowledge of the intensity function in real data, the prediction error of the conditional intensity is unavailable. Here we report the average log-likelihood for the real data, which have been widely adopted as a major evaluation metric in the related works [10, 16, 25–27, 30]; the higher the log-likelihood, the better the model fits.

4.1 Experimental setting and baseline methods

Now we describe the experiment configurations: We set the rank $R = 5$ in our setting. We consider the shared network that summarizes input data into a hidden embedding to be a fully connected three-layer network and the sub-network to be a fully connected single-layer network. The width of the hidden layers in the shared network is $n = 128$, and the width of the input layers in sub-networks (or the output layer in the shared network) is $p = 10$. We adopt the SoftPlus $f(x) = 1/\log(1 + \exp(x))$ as the activation function of each layer in the network. To learn the model’s parameters, we adopt the stochastic gradient descent method with a constant learning rate of 10^{-2} and the batch size is 32. All experiments are performed on Google Colaboratory (Pro version) with 12GB RAM and dual-core Intel processors, which speed up to 2.3 GHz (without GPU). Our code is available on Github¹.

This study considers three baseline methods: (1) Standard Hawkes process with an exponentially decaying kernel function (**Hawkes**): it specifies the conditional intensity function as $\lambda(t) = \mu + \alpha \sum_{t_j < t} \beta \exp\{-\beta(t - t_j)\}$, where parameters μ, α, β can be estimated via maximizing likelihood [6]; (2) Recurrent marked temporal point processes (**RMTPP**): it assumes the conditional intensity function $\lambda(t) = \exp(\mathbf{v}^\top \mathbf{h}_j + \omega(t - t_j) + b)$, where the j -th hidden state \mathbf{h}_j in the RNN represents the history influence up to the nearest happened event j , and $w(t - t_j)$ represents the current influence; the \mathbf{v}, ω, b are trainable parameters [4]; and (3) Neural Hawkes process (**NH**): it specifies the conditional intensity function as $\lambda^*(t) = f(\mathbf{v}^\top \mathbf{h}_t)$, where \mathbf{h}_t is the hidden state of a continuous-time LSTM up to time t representing the history influence, and the $f(\cdot)$ is a SoftPlus function

¹<https://github.com/meowoodie/Neural-Spectral-Marked-Point-Processes>

Algorithm 3: Efficient thinning algorithm for simulating point process

```
input  $\theta, T, \mathcal{M}$ ;  
output A set of events  $\mathcal{H}_t$  ordered by time.;  
Initialize  $\mathcal{H}_t = \emptyset, t = 0, m \sim \text{uniform}(\mathcal{M})$ ;  
while  $t < T$  do  
    Sample  $u \sim \text{uniform}(0, 1)$ ;  $m \sim \text{uniform}(\mathcal{M})$ ;  $D \sim \text{uniform}(0, 1)$ ;  
     $x' \leftarrow (t, m')$ ;  $\bar{\lambda} \leftarrow \lambda(x'|\mathcal{H}_t)$ ;  
     $t \leftarrow t - \ln u/\bar{\lambda}$ ;  
     $x \leftarrow (t, m)$ ;  $\tilde{\lambda} \leftarrow \lambda(x|\mathcal{H}_t)$ ;  
    if  $D\bar{\lambda} > \tilde{\lambda}$  then  
        |  $\mathcal{H}_t \leftarrow \mathcal{H}_t \cup \{(t, m)\}$ ;  $m' \leftarrow m$ ;  
    end  
end
```

which ensure the positive output given any input [10].

We note that, unlike the standard Hawkes process and our NSMPP, RMTTP and NH do not parameterize the kernel function directly; instead, they aim to model the conditional intensity using an LSTM-based structure. Particularly, these models pass the history information sequentially via a hidden state, where the recent memory will override the long-term memory. This has led RMTTP and NH to “overemphasize” the recent events and therefore assume the temporal correlation would monotonically decrease over time. In addition, RMTTP and NH can only deal with one-dimensional categorical marks, while our model can be extended to high-dimensional continuous mark space. To ensure comparability, we only consider one- and two-dimensional event consisting of time and mark in our experiment ($d \in \{1, 2\}$). For RMTTP and NH, the event’s mark will be discretized and treated as categorical input.

Synthetic data. We first discuss three one-dimensional and three two-dimensional synthetic data sets we used in this paper, which are simulated by the model described in Section 2.2 with randomly initialized parameters. We assume the background rate is a constant ($\mu = 1$) and only focus on recovering non-stationary kernel structures.

The simulation is carried out by thinning algorithm, which is a standard way to generate events from a point process [3, 5]. However, the vanilla thinning algorithm suffers from low sampling efficiency as it needs to sample in the space \mathcal{X} uniformly with the upper limit of the conditional intensity $\bar{\lambda}$ and only very few candidate points will be retained in the end. To improve sampling efficiency, we use an efficient thinning algorithm summarized in Algorithm 3. The “proposal” density is a heterogeneous MTPP, whose intensity function is defined from the previous iterations. This analogous to the idea of rejection sampling [13].

Figure 2 and Figure 3 present two examples for the one- and two-dimensional data sets, respectively. We fit our proposed model using 80% of the synthetic data set and take the rest of 20% as the testing set. Each data set is composed of 1,000 event sequences with an averaged

length of 121. For ease of comparison, we normalize the time and mark spaces for all the data sets to the range from 0 to 100.

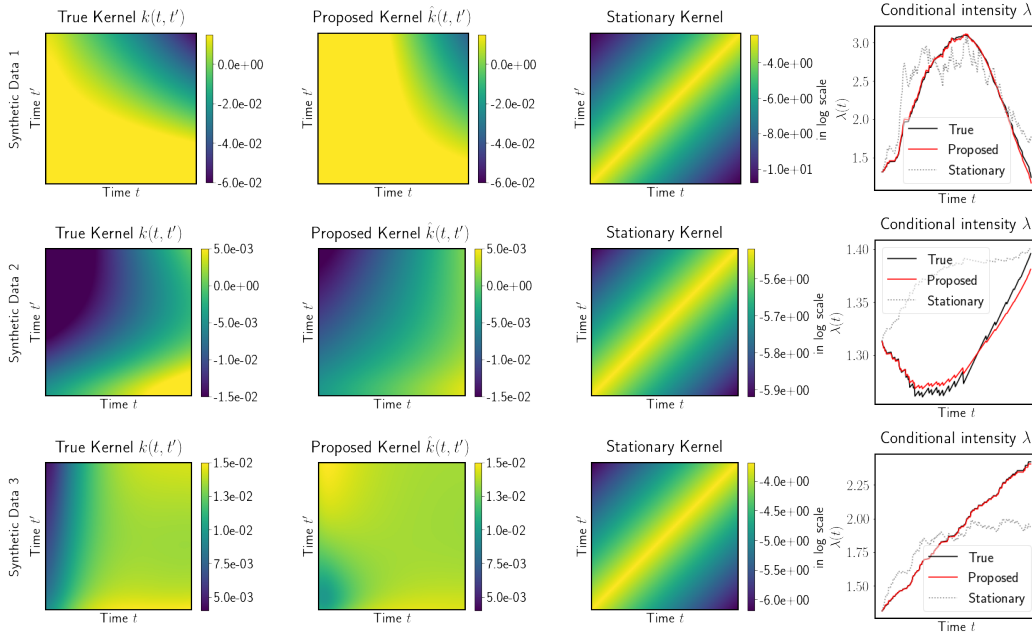


Figure 2: Examples of the recovered kernel on three one-dimensional synthetic data sets. The 1st column shows the true kernel that is used to generate the synthetic data set; the second column shows the learned kernel using our model; the 3rd column shows the learned kernel using the standard column process with a stationary kernel; the fourth column shows the corresponding predicted conditional intensity function given a sequence randomly selected from the data set. As we can observe, our model can better recover the structure of the true kernel and predict the conditional intensity function more accurately.

Kernel recovery. We examine our model’s ability to recover the true kernel. Figure 2 reports an example of the one-dimensional synthetic results. We observe that our proposed model can evidently recover the complex two-dimensional structure of the true kernel. In contrast, the standard Hawkes process with a stationary kernel failed to capture such non-stationarity. We emphasize that recovering kernel structure in this problem is exceedingly challenging since we do not assume the kernel structure and only observe discrete points in the one-dimensional data space.

We also extend our model to two-dimensional cases, where a continuous one-dimensional mark is introduced to the events. Figure 3 gives a few examples of the recovered kernel in a two-dimensional event space, including three snapshots of some two-dimensional “slices” of the four-dimensional kernel evaluation. We note that event points are sparsely scattered in the two-dimensional marked-temporal space, where the events’ correlation is measured in a high-dimensional (in our example, four-dimensional) kernel space. This makes the problem even more difficult compared to the one-dimensional case. The result shows that our model can still recover the kernel structure

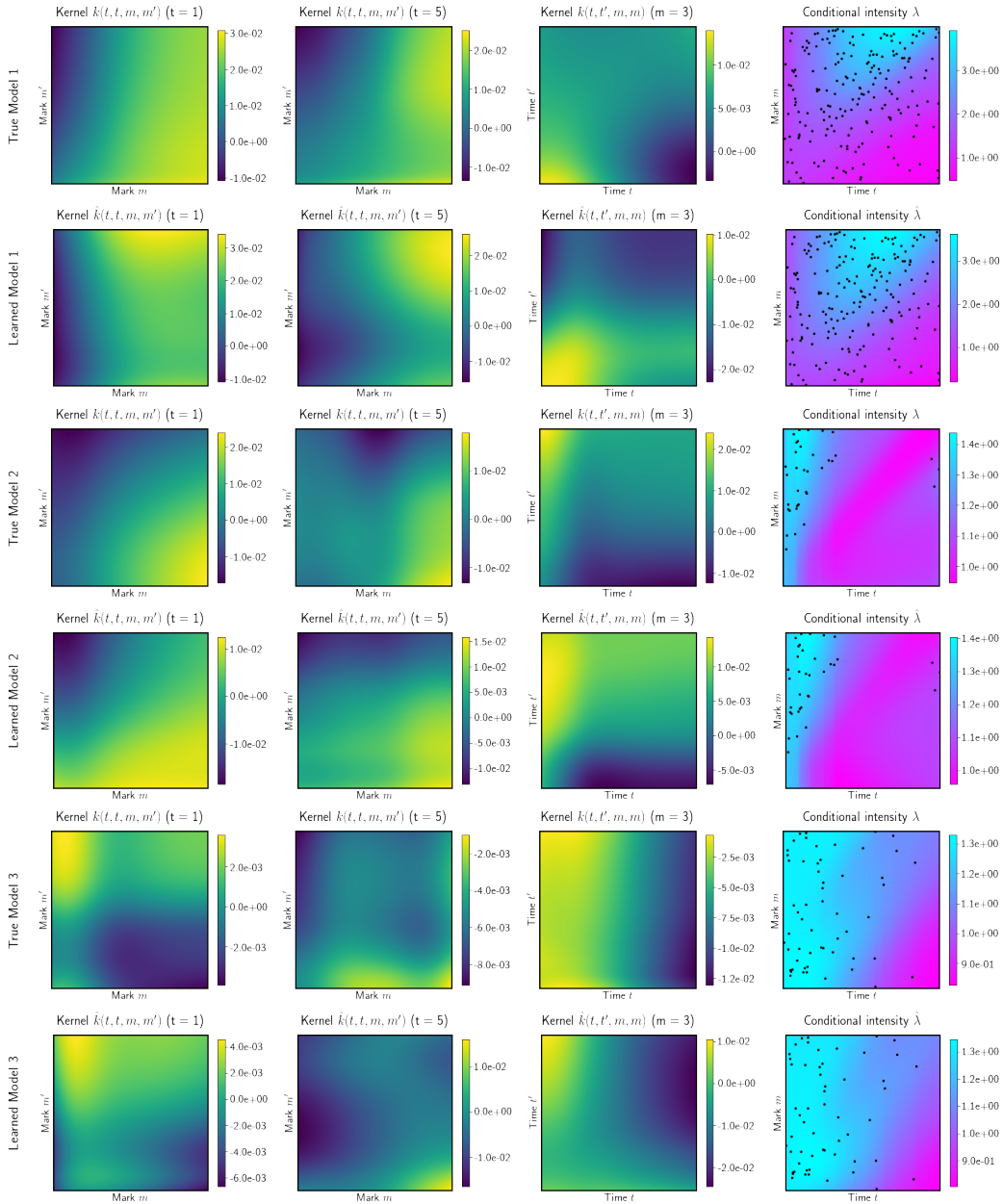


Figure 3: Example of the recovered kernel on three two-dimensional synthetic data sets. The 1st, 3rd, and fifth rows show the true model used to generate the synthetic data; the second, fourth, and sixth rows show the learned model using the same data sets. The first three columns present examples of kernel evaluation for the true and learned model; the last column shows the conditional intensity over marked-temporal space given one of the generated sequences, where the black dots indicate the location of the events. We can observe that our model can recover the four-dimensional kernel structure and predict the true conditional intensity accurately.

at different regions of the kernel space, even for the region where no data point appears (e.g., $k(t, t, m, m')$ would never be evaluated since we assume there is no two points occurred at the same time).

Intensity prediction. We evaluate the predictive accuracy for conditional intensity λ between our model and baseline methods. As an example, the last column in Figure 2 showcases the predicted one-dimensional conditional intensity functions given a sequence randomly selected from the testing set, using our method and a Hawkes model with the stationary kernel. The result shows that the predicted conditional intensity suggested by our model nearly flawlessly matches the ground truth. This confirms that our proposed model can capture the temporal dynamics accurately. In contrast, the Hawkes model with the stationary kernel only provides very limited flexibility in representing such complex temporal dependence. Two panels in the last column of Figure 3 give another comparison between the true and predicted two-dimensional conditional intensities over marked-temporal space. It further confirms that our model can also accurately predict the two-dimensional conditional intensity function, which is much more complicated than its one-dimensional counterpart.

We also conduct the same experiments on the rest of the synthetic data sets. Figure 4 visualize the true conditional intensities (solid black lines) and their predictions using each method. We observe that our method obtained much better predictive performances compared to other baseline approaches. Table 1 summarizes two other quantitative evaluation metrics for these methods: the average log-likelihood per sequence and mean absolute error (MAE) of the predicted conditional intensity. The result shows that our method greatly outperforms other baseline approaches in both metrics. In particular, the MAE of our method is at least 90% lower than the other methods for both one- and two-dimensional data sets.

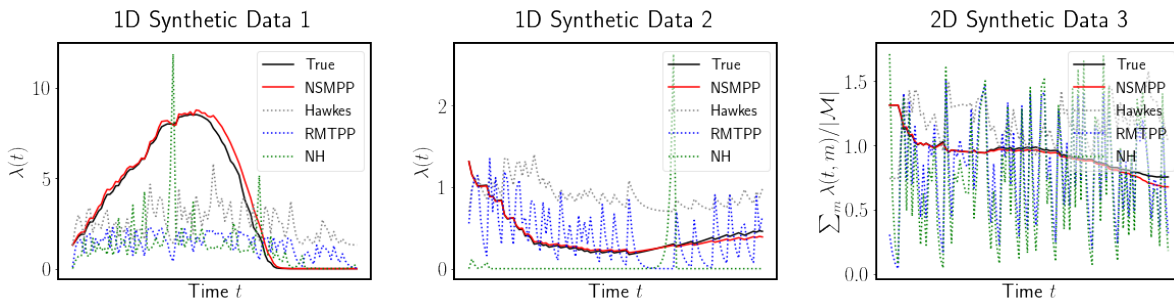


Figure 4: Predicted conditional intensity using our method and other baseline approaches for synthetic data sets. The results compare their predicted conditional intensity functions of the same sequence randomly selected from the testing set of a synthetic data set, which has been used to train these models. We aggregate the conditional intensity in mark space for ease of presentation and visualize the mean conditional intensity over time for two-dimensional synthetic data in the third panel.

Table 1: Performance comparison of our method and other baseline approaches.

ℓ / MAE ¹	1D Synthetic 1	1D Synthetic 2	1D Synthetic 3	2D Synthetic 1	2D Synthetic 2	2D Synthetic 3	Earthquake (2D)	Robbery (1D)
NSMPP	-17.68 / 0.24	-14.17 / 0.02	-21.94 / 0.02	-65.92 / 10.16	-87.02 / 0.20	-91.12 / 0.31	-56.50 / NA	-74.47 / NA
RMTPP	-29.84 / 3.27	-36.10 / 0.33	-89.56 / 0.34	-236.32 / 98.32	-320.01 / 20.97	-456.92 / 29.18	-218.39 / NA	-132.55 / NA
Neural Hawkes	-48.34 / 3.42	-52.97 / 0.41	-60.10 / 0.44	-289.10 / 49.21	-219.74 / 12.45	-420.00 / 28.99	-189.39 / NA	-96.10 / NA
Hawkes	-24.12 / 2.65	-77.36 / 0.52	-61.46 / 0.25	NA / NA	NA / NA	NA / NA	NA / NA	-197.84 / NA

¹ Each table’s entry includes the average log-likelihood per sequence (ℓ) and the mean absolute error (MAE) of the predicted conditional intensity on the corresponding data set.

Real-data results. Finally, we test our method on two large-scale real data sets: (1) *Atlanta 911 calls-for-service data*. The Atlanta Police Department provides the 911 calls-for-service data in Atlanta from the end of 2015 to 2017. We extract 7,831 reported robberies from the data set since robbers usually follow particular *modus operandi* (M.O.), where criminal times tend to have a causal relationship with each other. Each robbery report is associated with a timestamp indicating when the robbery occurred. We consider each series of robberies as a sequence. (2) *Northern California seismic data*. The Northern California Earthquake Data Center (NCEDC) provides public time series data [12] that comes from broadband, short period, strong motion seismic sensors, GPS, and other geophysical sensors. We extract 16,401 seismic records with a magnitude larger than 3.0 from 1978 to 2018 in Northern California and partition the data into multiple sequences every quarter. In Table 1, we report the log-likelihood of each method on the real data since the ground truth is not available. We can see that our model attains the highest log-likelihood value for both two real data set, indicating that our model is superior to other approaches on the real data sets.

5 Discussions

This paper presents a new marked point process model with a general kernel. Motivated by spectral decomposition of the kernel, we represent a general influence kernel using feature functions parameterized by neural networks and thus can capture complex dependence across spatial, temporal, and mark spaces. The model can be learned efficiently with theoretical performance guarantees. Our new kernel design has shown great promise in various application scenarios such as Gaussian processes kernel design. A limitation of our model is that when extending to high-dimensional mark space, the computation of log-likelihood can be expensive; adopting alternative training objectives (such as least-square) may potentially address this issue.

Acknowledgement

The works of S.Z., H.W., and Y.X. are supported by National Science Foundation (NSF) CAREER Award, CCF CCF-1650913, DMS-1830210, DMS-1938106. The work of X.C. is partially supported by the Alfred P. Sloan Foundation.

References

- [1] Martin Arjovsky and Léon Bottou. Towards principled methods for training generative adversarial networks. *arXiv preprint arXiv:1701.04862*, 2017.
- [2] Denny Britz, Anna Goldie, Minh-Thang Luong, and Quoc Le. Massive exploration of neural machine translation architectures. *arXiv preprint arXiv:1703.03906*, 2017.
- [3] D. J. Daley and D. Vere-Jones. *An introduction to the theory of point processes. Vol. II. Probability and its Applications* (New York). Springer, New York, second edition, 2008. General theory and structure.
- [4] Nan Du, Hanjun Dai, Rakshit Trivedi, Utkarsh Upadhyay, Manuel Gomez-Rodriguez, and Le Song. Recurrent marked temporal point processes: Embedding event history to vector. In *Proceedings of the 22nd ACM SIGKDD International Conference on Knowledge Discovery and Data Mining*, KDD '16, pages 1555–1564, New York, NY, USA, 2016. Association for Computing Machinery.
- [5] Edith Gabriel, Barry Rowlingson, and Peter Diggle. stpp: An r package for plotting, simulating and analyzing spatio-temporal point patterns. *Journal of Statistical Software*, 53:1–29, 04 2013.
- [6] Alan G. Hawkes. Spectra of some self-exciting and mutually exciting point processes. *Biometrika*, 58(1):83–90, 04 1971.
- [7] Sepp Hochreiter and Jürgen Schmidhuber. Long short-term memory. *Neural Comput.*, 9(8):1735–1780, November 1997.
- [8] Shuang Li, Shuai Xiao, Shixiang Zhu, Nan Du, Yao Xie, and Le Song. Learning temporal point processes via reinforcement learning. In *Proceedings of the 32nd International Conference on Neural Information Processing Systems*, NIPS '18, pages 10804–10814, Red Hook, NY, USA, 2018. Curran Associates Inc.
- [9] Minh-Thang Luong, Hieu Pham, and Christopher D Manning. Effective approaches to attention-based neural machine translation. *arXiv preprint arXiv:1508.04025*, 2015.
- [10] Hongyuan Mei and Jason M Eisner. The neural hawkes process: A neurally self-modulating multivariate point process. In *Advances in Neural Information Processing Systems 30*, pages 6754–6764. Curran Associates, Inc., 2017.
- [11] Song Mei, Andrea Montanari, and Phan-Minh Nguyen. A mean field view of the landscape of two-layer neural networks. *Proceedings of the National Academy of Sciences*, 115(33):E7665–E7671, 2018.
- [12] Northern California Earthquake Data Center. UC Berkeley Seismological Laboratory. Dataset. NCEDC, 2014.
- [13] Yosihiko Ogata. On lewis' simulation method for point processes. *IEEE Transactions on Information Theory*, 27(1):23–31, January 1981.
- [14] Yosihiko Ogata. Statistical models for earthquake occurrences and residual analysis for point processes. *Journal of the American Statistical association*, 83(401):9–27, 1988.
- [15] Yosihiko Ogata. Space-time point-process models for earthquake occurrences. *Annals of the Institute of Statistical Mathematics*, 50(2):379–402, 1998.

- [16] Takahiro Omi, naonori ueda, and Kazuyuki Aihara. Fully neural network based model for general temporal point processes. In *Advances in Neural Information Processing Systems 32*, pages 2120–2129. Curran Associates, Inc., 2019.
- [17] Alex Reinhart. A review of self-exciting spatio-temporal point processes and their applications. 2017.
- [18] Sami Remes, Markus Heinonen, and Samuel Kaski. Non-stationary spectral kernels. *arXiv preprint arXiv:1705.08736*, 2017.
- [19] Sami Remes, Markus Heinonen, and Samuel Kaski. Neural non-stationary spectral kernel. *arXiv preprint arXiv:1811.10978*, 2018.
- [20] Utkarsh Upadhyay, Abir De, and Manuel Gomez Rodriguez. Deep reinforcement learning of marked temporal point processes. In S. Bengio, H. Wallach, H. Larochelle, K. Grauman, N. Cesa-Bianchi, and R. Garnett, editors, *Advances in Neural Information Processing Systems 31*, pages 3168–3178. Curran Associates, Inc., 2018.
- [21] Ashish Vaswani, Noam Shazeer, Niki Parmar, Jakob Uszkoreit, Llion Jones, Aidan N Gomez, Łukasz Kaiser, and Illia Polosukhin. Attention is all you need. In *Advances in Neural Information Processing Systems 30*, pages 5998–6008. Curran Associates, Inc., 2017.
- [22] Halbert White. Maximum likelihood estimation of misspecified models. *Econometrica: Journal of the econometric society*, pages 1–25, 1982.
- [23] Shuai Xiao, Mehrdad Farajtabar, Xiaojing Ye, Junchi Yan, Le Song, and Hongyuan Zha. Wasserstein learning of deep generative point process models. In *Proceedings of the 31st International Conference on Neural Information Processing Systems, NIPS '17*, pages 3250–3259, Red Hook, NY, USA, 2017. Curran Associates Inc.
- [24] Shuai Xiao, Junchi Yan, Xiaokang Yang, Hongyuan Zha, and Stephen M. Chu. Modeling the intensity function of point process via recurrent neural networks. In *Proceedings of the Thirty-First AAAI Conference on Artificial Intelligence, AAAI '17*, pages 1597–1603. AAAI Press, 2017.
- [25] Qiang Zhang, Aldo Lipani, Omer Kirnap, and Emine Yilmaz. Self-attentive hawkes processes, 2019.
- [26] Shixiang Zhu, Ruyi Ding, Minghe Zhang, Pascal Van Hentenryck, and Yao Xie. Spatio-temporal point processes with attention for traffic congestion event modeling. *IEEE Transactions on Intelligent Transportation Systems*, 2021.
- [27] Shixiang Zhu, Shuang Li, Zhigang Peng, and Yao Xie. Imitation learning of neural spatio-temporal point processes. *IEEE Transactions on Knowledge and Data Engineering*, 2021.
- [28] Shixiang Zhu, Henry Shaowu Yuchi, Minghe Zhang, and Yao Xie. Sequential adversarial anomaly detection for one-class event data. *arXiv preprint arXiv:1910.09161*, 2019.
- [29] Shixiang Zhu, Henry Shaowu Yuchi, Minghe Zhang, and Yao Xie. Sequential adversarial anomaly detection with deep fourier kernel. In *ICASSP 2021-2021 IEEE International Conference on Acoustics, Speech and Signal Processing (ICASSP)*, pages 3345–3349. IEEE, 2021.
- [30] Shixiang Zhu, Minghe Zhang, Ruyi Ding, and Yao Xie. Deep fourier kernel for self-attentive point processes. In Arindam Banerjee and Kenji Fukumizu, editors, *Proceedings of The 24th International Conference on Artificial Intelligence and Statistics*, volume 130 of *Proceedings of Machine Learning Research*, pages 856–864. PMLR, 13–15 Apr 2021.
- [31] Simiao Zuo, Haoming Jiang, Zichong Li, Tuo Zhao, and Hongyuan Zha. Transformer hawkes process. In *International Conference on Machine Learning*, pages 11692–11702. PMLR, 2020.

A Proofs

A.1 Proof of Lemma 3.1

Proof of Lemma 3.1. For the j -th trajectory, define $\ell_j[k]$ as

$$\ell_j[k] = \int_{\mathcal{X}} \log \lambda_j[k](x) d\mathbb{N}_j(x) - \int_{\mathcal{X}} \lambda_j[k](x) dx, \quad (11)$$

then $\ell[k] = \frac{1}{M} \sum_j \ell_j[k]$. Let $\lambda_j^* = \lambda_j[k^*]$, $\tilde{\lambda}_j = \lambda_j[\tilde{k}]$, where the conditional intensity $\lambda[k]$ is defined as in (2), k^* and \tilde{k} are the true kernel and the perturbed one respectively. Then we have

$$\ell_j[\tilde{k}] - \ell_j[k^*] = \int_{\mathcal{X}} (\log \tilde{\lambda}_j(x) - \log \lambda_j^*(x)) d\mathbb{N}_j(x) - \int_{\mathcal{X}} (\tilde{\lambda}_j(x) - \lambda_j^*(x)) dx \quad (12)$$

By (2), $\lambda_j[k]$ is linear with respect to perturbation in k , that is,

$$\lambda_j[k](x) = \nu + \int_{\mathcal{X}_{t(x)}} k(x', x) d\mathbb{N}_j(x').$$

We then have that

$$\tilde{\lambda}_j(x) - \lambda_j^*(x) = \int_{\mathcal{X}_{t(x)}} (\tilde{k}(x', x) - k^*(x', x)) d\mathbb{N}_j(x') = \delta\lambda_j(x), \quad (13)$$

where the last equality is by definition of $\delta\lambda_j$.

Back to (12), the second term

$$\int_{\mathcal{X}} (\tilde{\lambda}_j(x) - \lambda_j^*(x)) dx = \int_{\mathcal{X}} \delta\lambda_j(x) dx; \quad (14)$$

The first term under Taylor expansion of log has that, for each $x \in \mathcal{X}$,

$$\log \tilde{\lambda}_j(x) - \log \lambda_j^*(x) = \frac{1}{\lambda_j^*(x)} \delta\lambda_j(x) - \frac{1}{2\xi_j(x)^2} (\delta\lambda_j(x))^2,$$

where $\xi_j(x)$ takes value between $\tilde{\lambda}_j(x)$ and $\lambda_j^*(x)$. By Assumption 3.1, both $\tilde{\lambda}_j(x)$ and $\lambda_j^*(x)$ are strictly positive and upper-bounded by c_2 , and thus $0 < \xi_j(x) \leq c_2$. This means that

$$\frac{1}{2\xi_j(x)^2} (\delta\lambda_j(x))^2 \geq \frac{1}{c_2^2} (\delta\lambda_j(x))^2, \quad \forall x \in \mathcal{X}.$$

Thus, the 1st term in (12) satisfies

$$\begin{aligned} \int_{\mathcal{X}} (\log \tilde{\lambda}_j(x) - \log \lambda_j^*(x)) d\mathbb{N}_j(x) &= \int_{\mathcal{X}} \delta\lambda_j(x) \frac{d\mathbb{N}_j(x)}{\lambda_j^*(x)} - \int_{\mathcal{X}} \frac{1}{2\xi_j(x)^2} (\delta\lambda_j(x))^2 d\mathbb{N}_j(x) \\ &\leq \int_{\mathcal{X}} \delta\lambda_j(x) \frac{d\mathbb{N}_j(x)}{\lambda_j^*(x)} - \frac{1}{2c_2^2} \int_{\mathcal{X}} (\delta\lambda_j(x))^2 d\mathbb{N}_j(x). \end{aligned} \quad (15)$$

Putting together (14) and (15),

$$\begin{aligned}\ell_j[\tilde{k}] - \ell_j[k^*] &\leq \int_{\mathcal{X}} \delta\lambda_j(x) \frac{d\mathbb{N}_j(x)}{\lambda_j^*(x)} - \frac{1}{2c_2^2} \int_{\mathcal{X}} (\delta\lambda_j(x))^2 d\mathbb{N}_j(x) - \int_{\mathcal{X}} \delta\lambda_j(x) dx \\ &= \int_{\mathcal{X}} \delta\lambda_j(x) \left(\frac{d\mathbb{N}_j(x)}{\lambda_j^*(x)} - dx \right) - \frac{1}{2c_2^2} \int_{\mathcal{X}} (\delta\lambda_j(x))^2 d\mathbb{N}_j(x).\end{aligned}$$

The above holds for each j , and taking the average over the M trajectories proves the lemma. \square

A.2 Proof of Theorem 3.2

Lemma A.1 (lower bound for KL-divergence). *Under Assumption 3.1,*

$$\mathbb{E} \left(\ell[k^*] - \ell[\tilde{k}] \right) \geq \frac{c_1^2}{2c_2^2} \exp(-(c_2 - c_1)|\mathcal{M}|T) \|\delta k\|_2^2,$$

holds true for any $\tilde{k} \in \bar{\mathcal{K}}$ and $\delta k = \tilde{k} - k^*$ (the ℓ_2 -norm is defined as (10).)

Proof. By Lemma 3.1, since all trajectories are i.i.d., and for each trajectory the conditional expectation

$$\mathbb{E} \left(\frac{d\mathbb{N}(x)}{\lambda[k^*](x)} \middle| \mathcal{H}_{t(x)} \right) = dx,$$

there is

$$\begin{aligned}\mathbb{E} \left(\ell[k^*] - \ell[\tilde{k}] \right) &\geq \mathbb{E} \left(\int_{\mathcal{X}} \delta\lambda(x) \left(\frac{d\mathbb{N}(x)}{\lambda[k^*](x)} - dx \right) + \frac{1}{2c_2^2} \int_{\mathcal{X}} (\delta\lambda(x))^2 d\mathbb{N}(x) \right) \\ &= \frac{1}{2c_2^2} \mathbb{E} \left(\int_{\mathcal{X}} (\delta\lambda(x))^2 d\mathbb{N}(x) \right).\end{aligned}$$

Following Assumption 3.1

$$\frac{1}{2c_2^2} \mathbb{E} \left(\int_{\mathcal{X}} (\delta\lambda(x))^2 d\mathbb{N}(x) \right) = \frac{1}{2c_2^2} \mathbb{E} \left(\int_{\mathcal{X}} (\delta\lambda(x))^2 \lambda[k^*](x) dx \right) \geq \frac{c_1}{2c_2^2} \mathbb{E} \left(\int_{\mathcal{X}} (\delta\lambda(x))^2 dx \right).$$

Next we lower bound the term above by taking the integral over the event space $\mathcal{E} = \bigsqcup_{i=0}^{\infty} \mathcal{E}_i$ of trajectories, where for each i ,

$$\mathcal{E}_i = \{(x_1, x_2, \dots, x_i) \in \mathcal{X}^i, t(x_1) < \dots < t(x_i)\} \subset \mathcal{X}^i$$

consists of all the trajectories with exactly i events. For each $\mathcal{H}_T \in \mathcal{E}$, let \mathbb{N} be the associated counting measure, the probability density of \mathcal{H}_T

$$\rho(\mathcal{H}_T) = \exp \left(\int_{\mathcal{X}} \log \lambda[k^*] d\mathbb{N}(x) - \int_{\mathcal{X}} \lambda[k^*](x) dx \right) \geq \exp(|\mathcal{H}_T| \log c_1 - |\mathcal{M}|T c_2) =: \underline{\rho}(\mathcal{H}_T).$$

Then if we ignore the temporal order of events,

$$\begin{aligned}
& \frac{c_1}{2c_2^2} \mathbb{E} \left(\int_{\mathcal{X}} (\delta\lambda(x))^2 dx \right) \\
& \geq \frac{c_1}{2c_2^2} \sum_{i=0}^{\infty} \int_{\mathcal{E}_i} \left(\int_{\mathcal{X}} (\delta\lambda(x))^2 dx \right) \underline{\rho}(\mathcal{H}_T) dx_1 dx_2 \cdots dx_i \\
& = \frac{c_1}{2c_2^2} \sum_{i=0}^{\infty} \frac{1}{i!} \int_{\mathcal{X}^i} \left(\int_{\mathcal{X}} (\delta\lambda(x))^2 dx \right) \underline{\rho}(\mathcal{H}_T) dx_1 dx_2 \cdots dx_i \\
& = \frac{c_1}{2c_2^2} \sum_{i=0}^{\infty} \frac{1}{i!} \int_{\mathcal{X}^i} \left(\int_{\mathcal{X}} \int_{\mathcal{X}_{t(x)}} \int_{\mathcal{X}_{t(x)}} \delta k(x', x) \delta k(x'', x) d\mathbb{N}(x') d\mathbb{N}(x'') dx \right) \underline{\rho}(\mathcal{H}_T) dx_1 dx_2 \cdots dx_i \\
& = \frac{c_1}{2c_2^2} \sum_{i=0}^{\infty} \frac{1}{i!} \int_{\mathcal{X}^i} \left(\int_{\mathcal{X}} \int_{\mathcal{X}_{t(x)}} \int_{\mathcal{X}_{t(x)}} \delta k(x', x) \delta k(x'', x) d\mathbb{N}(x') d\mathbb{N}(x'') dx \right) \underline{\rho}(\mathcal{H}_T) dx_1 dx_2 \cdots dx_i \\
& = \frac{c_1}{2c_2^2} \sum_{i=0}^{\infty} \frac{1}{i!} \int_{\mathcal{X}} \int_{\mathcal{X}_{t(x)}} \int_{\mathcal{X}_{t(x)}} \int_{\mathcal{X}^i} \delta k(x', x) \delta k(x'', x) \underline{\rho}(\mathcal{H}_T) dx_1 dx_2 \cdots dx_i d\mathbb{N}(x') d\mathbb{N}(x'') dx
\end{aligned}$$

For $x' \neq x''$, $d\mathbb{N}(x')d\mathbb{N}(x'') = 1$ when two of x_1, \dots, x_i equal to x', x'' . For $x' = x''$, $d\mathbb{N}(x')d\mathbb{N}(x'') = 1$ when one of x_1, \dots, x_i equals to $x' = x''$. So

$$\begin{aligned}
& \frac{c_1}{2c_2^2} \mathbb{E} \left(\int_{\mathcal{X}} (\delta\lambda(x))^2 dx \right) \\
& \geq \frac{c_1}{2c_2^2} \sum_{i=0}^{\infty} \frac{1}{i!} \int_{\mathcal{X}} \int_{\mathcal{X}_{t(x)}} \int_{\mathcal{X}_{t(x)}} \int_{\mathcal{X}^i} \delta k(x', x) \delta k(x'', x) \underline{\rho}(\mathcal{H}_T) dx_1 dx_2 \cdots dx_i d\mathbb{N}(x') d\mathbb{N}(x'') dx \\
& = \frac{c_1}{2c_2^2} \sum_{i=2}^{\infty} \frac{i(i-1)}{i!} \int_{\mathcal{X}} \int_{\mathcal{X}_{t(x)}} \int_{\mathcal{X}_{t(x)}} \int_{\mathcal{X}^{i-2}} \delta k(x', x) \delta k(x'', x) \underline{\rho}(\mathcal{H}_T) dx_3 \cdots dx_i dx' dx'' dx \\
& \quad + \frac{c_1}{2c_2^2} \sum_{i=1}^{\infty} \frac{i}{i!} \int_{\mathcal{X}} \int_{\mathcal{X}_{t(x)}} \int_{\mathcal{X}^{i-1}} \delta k(x', x) \delta k(x', x) \underline{\rho}(\mathcal{H}_T) dx_2 \cdots dx_i dx' dx \\
& = \frac{c_1}{2c_2^2} \sum_{i=2}^{\infty} \frac{i(i-1)}{i!} \int_{\mathcal{X}} \int_{\mathcal{X}_{t(x)}} \int_{\mathcal{X}_{t(x)}} \delta k(x', x) \delta k(x'', x) |\mathcal{M}|^{i-2} T^{i-2} c_1^i \exp(-c_2 |\mathcal{M}| T) dx' dx'' dx \\
& \quad + \frac{c_1}{2c_2^2} \sum_{i=1}^{\infty} \frac{i}{i!} \int_{\mathcal{X}} \int_{\mathcal{X}_{t(x)}} \delta k(x', x) \delta k(x', x) |\mathcal{M}|^{i-1} T^{i-1} c_1^i \exp(-c_2 |\mathcal{M}| T) dx' dx \\
& = \frac{c_1}{2c_2^2} \sum_{i=2}^{\infty} \frac{i(i-1)}{i!} \int_{\mathcal{X}} |\mathcal{M}|^{i-2} T^{i-2} c_1^i \exp(-c_2 |\mathcal{M}| T) \left(\int_{\mathcal{X}_{t(x)}} \delta k(x', x) dx' \right)^2 dx \\
& \quad + \frac{c_1}{2c_2^2} \int_{\mathcal{X}} \int_{\mathcal{X}_{t(x)}} \delta k(x', x) \delta k(x', x) \sum_{i=1}^{\infty} \frac{1}{(i-1)!} |\mathcal{M}|^{i-1} T^{i-1} c_1^i \exp(-c_2 |\mathcal{M}| T) dx' dx \\
& \geq \frac{c_1}{2c_2^2} \int_{\mathcal{X}} \int_{\mathcal{X}_{t(x)}} \delta k(x', x) \delta k(x', x) \sum_{i=1}^{\infty} \frac{1}{(i-1)!} |\mathcal{M}|^{i-1} T^{i-1} c_1^i \exp(-c_2 |\mathcal{M}| T) dx' dx
\end{aligned}$$

$$\begin{aligned}
&= \frac{c_1^2}{2c_2^2} \int_{\mathcal{X}} \int_{\mathcal{X}_{t(x)}} \delta k(x', x) \delta k(x', x) \exp(-(c_2 - c_1)|\mathcal{M}|T) dx' dx \\
&= \frac{c_1^2}{2c_2^2} \exp(-(c_2 - c_1)|\mathcal{M}|T) \|\delta k\|_2^2.
\end{aligned}$$

□

Proof of Theorem 3.2. This follows immediately from Lemma A.1. □

A.3 Proof of Theorem 3.3

Lemma A.2. *Under Assumption 3.1, for any $k \in \bar{\mathcal{K}}$,*

$$\mathbb{E}(\ell[k^*] - \ell[k]) \leq \frac{c_2^3 |\mathcal{M}|T + c_2^2}{2c_1^2} \exp((c_2 - c_1)|\mathcal{M}|T) \|k - k^*\|_2^2,$$

Proof. Similar to the proof of Lemma 3.1 and Theorem 3.2, for a single trajectory and any $k \in \bar{\mathcal{K}}$ let

$$\begin{aligned}
\delta k(x', x) &= k(x', x) - k^*(x', x), \forall x', x \in \mathcal{X}, t(x') < t(x), \\
\delta \lambda(x) &= \int_{\mathcal{X}_{t(x)}} \delta k(x', x) d\mathbb{N}(x').
\end{aligned}$$

There is

$$\begin{aligned}
\ell[k^*] - \ell[k] &= \int_{\mathcal{X}} \delta \lambda(x) dx - \int_{\mathcal{X}} \log \left(\frac{\lambda[k](x)}{\lambda[k^*](x)} \right) d\mathbb{N}(x) \\
&= \int_{\mathcal{X}} \delta \lambda(x) dx - \int_{\mathcal{X}} \log \left(1 + \frac{\delta \lambda(x)}{\lambda[k^*](x)} \right) d\mathbb{N}(x) \\
&= \int_{\mathcal{X}} \delta \lambda(x) \left(dx - \frac{d\mathbb{N}(x)}{\lambda[k^*](x)} \right) + \frac{1}{2} \frac{\delta \lambda(x)^2}{\bar{\lambda}(x)^2} d\mathbb{N}(x),
\end{aligned}$$

for some $\bar{\lambda}(x)$ determined by $\mathcal{H}_{t(x)}$ such that $\bar{\lambda}(x)$ is in between $\lambda[k^*](x)$ and $\lambda[k](x)$ for all $x \in \mathcal{X}$. Then

$$\begin{aligned}
\mathbb{E}(\ell[k^*] - \ell[k]) &\leq \mathbb{E} \left(\int_{\mathcal{X}} \frac{1}{2} \frac{\delta \lambda(x)^2}{\bar{\lambda}(x)^2} d\mathbb{N}(x) \right) \\
&= \mathbb{E} \left(\int_{\mathcal{X}} \frac{1}{2} \frac{\delta \lambda(x)^2}{\bar{\lambda}(x)^2} \lambda[k^*](x) dx \right) \\
&\leq \frac{c_2}{2c_1^2} \mathbb{E} \left(\int_{\mathcal{X}} \delta \lambda(x)^2 dx \right).
\end{aligned}$$

For each trajectory $\mathcal{H}_T \in \mathcal{E}$, the probability density of \mathcal{H}_T

$$\rho(\mathcal{H}_T) = \exp \left(\int_{\mathcal{X}} \log \lambda[k^*](x) d\mathbb{N}(x) - \int_{\mathcal{X}} \lambda[k^*](x) dx \right) \leq \exp(|\mathcal{H}_T| \log c_2 - |\mathcal{M}|T c_1) =: \bar{\rho}(\mathcal{H}_T).$$

$$\begin{aligned}
\mathbb{E}(\ell[k^*] - \ell[k]) &\leq \frac{c_2}{2c_1^2} \mathbb{E} \left(\int_{\mathcal{X}} \delta\lambda(x)^2 dx \right) \\
&\leq \frac{c_2}{2c_1^2} \sum_{i=0}^{\infty} \int_{\mathcal{E}_i} \left(\int_{\mathcal{X}} \delta\lambda(x)^2 dx \right) \bar{\rho}(\mathcal{H}_T) dx_1 \cdots dx_i \\
&= \frac{c_2}{2c_1^2} \sum_{i=2}^{\infty} \frac{1}{(i-2)!} \int_{\mathcal{X}} |\mathcal{M}|^{i-2} T^{i-2} c_2^i \exp(-c_1 |\mathcal{M}| T) \left(\int_{\mathcal{X}_{t(x)}} \delta k(x', x) dx' \right)^2 dx \\
&\quad + \frac{c_2}{2c_1^2} \int_{\mathcal{X}} \int_{\mathcal{X}_{t(x)}} \delta k(x', x)^2 \sum_{i=1}^{\infty} \frac{1}{(i-1)!} |\mathcal{M}|^{i-1} T^{i-1} c_2^i \exp(-c_1 |\mathcal{M}| T) dx' dx \\
&= \frac{c_2}{2c_1^2} \int_{\mathcal{X}} c_2^2 \exp((c_2 - c_1) |\mathcal{M}| T) \left(\int_{\mathcal{X}_{t(x)}} \delta k(x', x) dx' \right)^2 dx \\
&\quad + \frac{c_2}{2c_1^2} \int_{\mathcal{X}} \int_{\mathcal{X}_{t(x)}} \delta k(x', x)^2 c_2 \exp((c_2 - c_1) |\mathcal{M}| T) dx' dx.
\end{aligned}$$

By Cauchy-Schwarz inequality,

$$\begin{aligned}
&\frac{c_2}{2c_1^2} \int_{\mathcal{X}} c_2^2 \exp((c_2 - c_1) |\mathcal{M}| T) \left(\int_{\mathcal{X}_{t(x)}} \delta k(x', x) dx' \right)^2 dx \\
&\leq \frac{c_2}{2c_1^2} \int_{\mathcal{X}} c_2^2 \exp((c_2 - c_1) |\mathcal{M}| T) |\mathcal{X}_{t(x)}| \int_{\mathcal{X}_{t(x)}} \delta k(x', x)^2 dx' dx \\
&\leq \frac{c_2}{2c_1^2} \int_{\mathcal{X}} c_2^2 \exp((c_2 - c_1) |\mathcal{M}| T) |\mathcal{M}| T \int_{\mathcal{X}_{t(x)}} \delta k(x', x)^2 dx' dx \\
&= \frac{c_2^3 |\mathcal{M}| T}{2c_1^2} \exp((c_2 - c_1) |\mathcal{M}| T) \|\delta k\|_2^2.
\end{aligned}$$

So together we have

$$\mathbb{E}(\ell[k^*] - \ell[k]) \leq \frac{c_2^3 |\mathcal{M}| T + c_2^2}{2c_1^2} \exp((c_2 - c_1) |\mathcal{M}| T) \|k - k^*\|_2^2,$$

□

Then we get back to the proof of Theorem 3.3.

Proof of Theorem 3.3. Let $A_0 \in \mathcal{A}_R$ be the one which minimizes $\|k^* - k_{A_0}\|_2$, i.e.,

$$\|k^* - k_{A_0}\|_2 = D(k^*, \mathcal{K}_{\text{finite}}).$$

By Lemma A.1 and Lemma A.2, there is

$$\begin{aligned}
&\frac{c_2^3 |\mathcal{M}| T + c_2^2}{2c_1^2} \exp((c_2 - c_1) |\mathcal{M}| T) D(k^*, \mathcal{K}_{\text{finite}})^2 \geq \mathbb{E}(\ell[k^*] - \ell[k_{A_0}]) \\
&\geq \mathbb{E}(\ell[k^*] - \ell[k_{\tilde{A}}]) \geq \frac{c_1^2}{2c_2^2} \exp(-(c_2 - c_1) |\mathcal{M}| T) \|k^* - k_{\tilde{A}}\|_2^2.
\end{aligned}$$

□

A.4 Proof of Theorem 3.4

Let $\bar{\mathcal{A}} = \{A \in \mathbb{R}^{S \times S}, k[A] \in \bar{\mathcal{K}}\}$. We prove the theorem under the following assumption:

Assumption A.1. Assume \tilde{A} is the unique minimizer in (9), is of rank exactly R , and $\text{vec}(\tilde{A})$ is on the interior of $\text{vec}(\bar{\mathcal{A}}) := \{\text{vec}(A) : A \in \bar{\mathcal{A}}\} \subseteq \mathbb{R}^{S^2}$.

Proof. Consider the local parametrization of \mathcal{A}_R in the neighborhood of \tilde{A} based on the singular value decomposition $\tilde{A} = U\Lambda V^T$, $U, V \in \mathbb{R}^{S \times R}$, Λ is a R -by- R diagonal matrix,

$$A = (U \bar{U}) \begin{pmatrix} \Lambda + P_1 & P_2^T \\ P_3 & P_3(\Lambda + P_1)^{-1}P_2^T \end{pmatrix} \begin{pmatrix} V^T \\ \bar{V}^T \end{pmatrix}.$$

Here $(U \bar{U}), (V \bar{V})$ are fixed orthogonal matrices where the first R columns are U, V respectively. $P_1 \in \mathbb{R}_{R \times R}, P_2, P_3 \in \mathbb{R}^{(S-R) \times R}$ are parameters in the neighborhood of 0 such that $\Lambda + P_1$ is non-singular. By Theorem 3.2 of [22], let $\hat{P}_{1,\text{MLE}}, \hat{P}_{2,\text{MLE}}, \hat{P}_{3,\text{MLE}}$ be the parameters which correspond to \hat{A}_{MLE} , i.e.

$$\hat{A}_{\text{MLE}} = (U \bar{U}) \begin{pmatrix} \Lambda + \hat{P}_{1,\text{MLE}} & \hat{P}_{2,\text{MLE}}^T \\ \hat{P}_{3,\text{MLE}} & \hat{P}_{3,\text{MLE}}(\Lambda + \hat{P}_{1,\text{MLE}})^{-1}\hat{P}_{2,\text{MLE}}^T \end{pmatrix} \begin{pmatrix} V^T \\ \bar{V}^T \end{pmatrix}.$$

For simplicity, let $p = (\text{vec}^T(P_1), \text{vec}^T(P_2), \text{vec}^T(P_3))^T$. Then

$$\sqrt{M}\hat{p}_{\text{MLE}} = \sqrt{M} \begin{pmatrix} \text{vec}(\hat{P}_{1,\text{MLE}}) \\ \text{vec}(\hat{P}_{2,\text{MLE}}) \\ \text{vec}(\hat{P}_{3,\text{MLE}}) \end{pmatrix} \xrightarrow{D} \mathcal{N}(0, I^{-1}JI^{-1}),$$

where

$$I = \mathbb{E} \left(\frac{\partial^2 \ell_A}{\partial p \partial p^T} \right) \Big|_{P_1=0, P_2=0, P_3=0},$$

$$J = \mathbb{E} \left(\frac{\partial \ell_A}{\partial p} \frac{\partial \ell_A}{\partial p^T} \right) \Big|_{P_1=0, P_2=0, P_3=0}.$$

For simplicity, from now on, we write all partial derivatives taken at $P_1 = 0, P_2 = 0, P_3 = 0, A = \tilde{A}$ without specifying the location. Let

$$\gamma = \text{vec}(A - \tilde{A}) - \frac{\partial \text{vec}(A)}{\partial p^T} p,$$

since $\|\gamma\| = O(\|p\|_2^2)$, there is

$$\sqrt{M}\gamma \xrightarrow{P} 0.$$

$$\sqrt{M}\text{vec}(\hat{A}_{\text{MLE}} - \tilde{A}) = \sqrt{M} \left(\gamma + \frac{\partial \text{vec}(A)}{\partial p^T} \hat{p}_{\text{MLE}} \right) \xrightarrow{D} \mathcal{N} \left(0, \frac{\partial \text{vec}(A)}{\partial p^T} I^{-1} J I^{-1} \frac{\partial \text{vec}^T(A)}{\partial p} \right).$$

Next we look at the covariance matrix of the multivariate Gaussian distribution,

$$\frac{\partial \ell_A}{\partial p} = \frac{\partial \text{vec}^T(A)}{\partial p} \frac{\partial \ell_A}{\partial \text{vec}(A)}.$$

Since \tilde{A} maximizes $\mathbb{E}(\ell_A)$ and is on the interior of $\bar{\mathcal{A}}$ and hence the interior of the manifold parametrized by p , we have

$$\mathbb{E}\left(\frac{\partial \ell_A}{\partial p}\right) = \frac{\partial \text{vec}^T(A)}{\partial p} \mathbb{E}\left(\frac{\partial \ell_A}{\partial \text{vec}(A)}\right) = \frac{\partial \text{vec}^T(A)}{\partial p} \text{vec}(\tilde{G}) = 0. \quad (16)$$

$$\begin{aligned} J &= \mathbb{E}\left(\frac{\partial \ell_A}{\partial p} \frac{\partial \ell_A}{\partial p^T}\right) \\ &= \frac{\partial \text{vec}^T(A)}{\partial p} \mathbb{E}\left(\frac{\partial \ell_A}{\partial \text{vec}(A)} \frac{\partial \ell_A}{\partial \text{vec}^T(A)}\right) \frac{\partial \text{vec}(A)}{\partial p^T} \\ &= \frac{\partial \text{vec}^T(A)}{\partial p} \left(\text{Cov}\left(\frac{\partial \ell_A}{\partial \text{vec}(A)}, \frac{\partial \ell_A}{\partial \text{vec}^T(A)}\right) + \mathbb{E}\left(\frac{\partial \ell_A}{\partial \text{vec}(A)}\right) \mathbb{E}\left(\frac{\partial \ell_A}{\partial \text{vec}^T(A)}\right)^T \right) \frac{\partial \text{vec}(A)}{\partial p^T} \\ &= \frac{\partial \text{vec}^T(A)}{\partial p} \tilde{J} \frac{\partial \text{vec}(A)}{\partial p^T}. \end{aligned}$$

For any $i, j \in [(2S - R)R]$,

$$\begin{aligned} \frac{\partial^2 \ell_A}{\partial p_i \partial p_j} &= \frac{\partial \text{vec}^T(A)}{\partial p_i} \frac{\partial^2 \ell_A}{\partial \text{vec}(A) \partial p_j} + \frac{\partial \text{vec}^T(A)}{\partial p_j \partial p_j} \frac{\partial \ell_A}{\partial \text{vec}(A)} \\ &= \frac{\partial \text{vec}^T(A)}{\partial p_i} \frac{\partial^2 \ell_A}{\partial \text{vec}(A) \partial \text{vec}^T(A)} \frac{\partial \text{vec}(A)}{\partial p_j} + \frac{\partial^2 \text{vec}^T(A)}{\partial p_j \partial p_j} \frac{\partial \ell_A}{\partial \text{vec}(A)}, \end{aligned}$$

the (i,j)-th component of I

$$I_{ij} = \mathbb{E}\left(\frac{\partial^2 \ell_A}{\partial p_i \partial p_j}\right) = \frac{\partial \text{vec}^T(A)}{\partial p_i} \tilde{I} \frac{\partial \text{vec}(A)}{\partial p_j} + \frac{\partial^2 \text{vec}^T(A)}{\partial p_j \partial p_j} \text{vec}(\tilde{G}).$$

We observe that some blocks of $(\frac{\partial^2 \text{vec}^T(A)}{\partial p_j \partial p_j} \text{vec}(\tilde{G}))_{ij}$ are 0.

$$\frac{\partial^2 \text{vec}^T(A) \text{vec}(\tilde{G})}{\partial \text{vec}(P_1) \partial \text{vec}^T(P_1)} = \frac{\partial^2 \text{vec}^T(UP_1V^T + UP_2^T\bar{V}^T + \bar{U}P_3V^T + \bar{U}P_3(\Lambda + P_1)^{-1}P_2^T\bar{V}^T) \text{vec}(\tilde{G})}{\partial \text{vec}(P_1) \partial \text{vec}^T(P_1)} = 0,$$

as (1) the second order derivative of $UP_1V^T, UP_2^T\bar{V}^T, \bar{U}P_3V^T$ over P_1 is 0 since they are either linear in or irrelevant with P_1 , (2) the second order derivative of $UP_1V^T + \bar{U}P_3(\Lambda + P_1)^{-1}P_2^T\bar{V}^T$ over P_1 is 0 since it is taken at $P_2 = P_3 = 0$. Also we have

$$\begin{aligned} \frac{\partial^2 \text{vec}^T(A) \text{vec}(\tilde{G})}{\partial \text{vec}(P_1) \partial \text{vec}^T(P_2)} &= 0, & \frac{\partial^2 \text{vec}^T(A) \text{vec}(\tilde{G})}{\partial \text{vec}(P_1) \partial \text{vec}^T(P_3)} &= 0, \\ \frac{\partial^2 \text{vec}^T(A) \text{vec}(\tilde{G})}{\partial \text{vec}(P_2) \partial \text{vec}^T(P_2)} &= 0, & \frac{\partial^2 \text{vec}^T(A) \text{vec}(\tilde{G})}{\partial \text{vec}(P_3) \partial \text{vec}^T(P_3)} &= 0, \end{aligned}$$

for similar reasons. The only non-zero block is

$$\begin{aligned}
\frac{\partial^2 \text{vec}^T(A) \text{vec}(\tilde{G})}{\partial \text{vec}(P_2) \partial \text{vec}^T(P_3)} &= \frac{\partial^2 \text{vec}^T(\bar{U} P_3 \Lambda^{-1} P_2^T \bar{V}^T) \text{vec}(\tilde{G})}{\partial \text{vec}(P_2) \partial \text{vec}^T(P_3)} \\
&= \frac{\partial}{\partial \text{vec}(P_2)} \frac{\partial \text{vec}^T(\bar{U} P_3 \Lambda^{-1} P_2^T \bar{V}^T) \text{vec}(\tilde{G})}{\partial \text{vec}^T(P_3)} \\
&= \frac{\partial}{\partial \text{vec}(P_2)} \frac{\partial \text{vec}^T(P_3) (\Lambda^{-1} P_2^T \bar{V}^T \otimes \bar{U}^T) \text{vec}(\tilde{G})}{\partial \text{vec}^T(P_3)} \\
&= \frac{\partial}{\partial \text{vec}(P_2)} ((\Lambda^{-1} P_2^T \bar{V}^T \otimes \bar{U}^T) \text{vec}(\tilde{G}))^T \\
&= \frac{\partial}{\partial \text{vec}(P_2)} \text{vec}^T(\bar{U}^T \tilde{G} \bar{V} P_2 \Lambda^{-1}) \\
&= \frac{\partial}{\partial \text{vec}(P_2)} \text{vec}^T(P_2) (\Lambda^{-1} \otimes \bar{V}^T \tilde{G}^T \bar{U}) \\
&= \Lambda^{-1} \otimes \bar{V}^T \tilde{G}^T \bar{U}.
\end{aligned}$$

So

$$I = \frac{\partial \text{vec}^T(A)}{\partial p} \tilde{I} \frac{\partial \text{vec}(A)}{\partial p^T} + \begin{pmatrix} 0 & 0 & 0 \\ 0 & 0 & \Lambda^{-1} \otimes \bar{V}^T \tilde{G}^T \bar{U} \\ 0 & \Lambda^{-1} \otimes \bar{U}^T \tilde{G} \bar{V} & 0 \end{pmatrix}.$$

At last, we compute $\partial \text{vec}(A) / \partial p^T$,

$$\begin{aligned}
\frac{\partial \text{vec}(A)}{\partial p^T} &= \begin{pmatrix} \frac{\partial \text{vec}(A)}{\partial \text{vec}^T(P_1)} & \frac{\partial \text{vec}(A)}{\partial \text{vec}^T(P_2)} & \frac{\partial \text{vec}(A)}{\partial \text{vec}^T(P_3)} \end{pmatrix} \\
&= \begin{pmatrix} \frac{\partial \text{vec}(U P_1 V^T)}{\partial \text{vec}^T(P_1)} & \frac{\partial \text{vec}(U P_2^T \bar{V}^T)}{\partial \text{vec}^T(P_2)} & \frac{\partial \text{vec}(\bar{U} P_3 V^T)}{\partial \text{vec}^T(P_3)} \end{pmatrix} \\
&= (V \otimes U \quad \bar{V} \otimes U \quad V \otimes \bar{U}).
\end{aligned}$$

Let

$$Z = \begin{pmatrix} \mathbb{I}_{R^2} & & \\ & Q_{R,S-R} & \\ & & \mathbb{I}_{R(S-R)} \end{pmatrix} \begin{pmatrix} V^T \otimes \mathbb{I}_R & \mathbb{I}_R \otimes U^T \\ \bar{V}^T \otimes \mathbb{I}_R & \\ & & \mathbb{I}_R \otimes \bar{U}^T \end{pmatrix},$$

Z has full row-rank, and

$$\frac{\partial \text{vec}(A)}{\partial p^T} Z = (V \otimes U \quad \bar{V} \otimes U \quad V \otimes \bar{U}) \begin{pmatrix} V^T \otimes \mathbb{I}_R & \mathbb{I}_R \otimes U^T \\ \bar{V}^T \otimes \mathbb{I}_R & \\ & & \mathbb{I}_R \otimes \bar{U}^T \end{pmatrix} = ((V V^T + \bar{V} \bar{V}^T) \otimes U \quad V \otimes (U U^T + \bar{U} \bar{U}^T)) = F.$$

Then the covariance matrix of the asymptotic distribution of $\text{vec}(\hat{A}_{\text{MLE}})$

$$\begin{aligned} \frac{\partial \text{vec}(A)}{\partial p^T} I^{-1} J I^{-1} \frac{\partial \text{vec}^T(A)}{\partial p} &= \frac{\partial \text{vec}(A)}{\partial p^T} Z (Z^T I Z)^\dagger Z^T J Z (Z^T I Z)^\dagger Z^T \frac{\partial \text{vec}^T(A)}{\partial p} \\ &= F (Z^T I Z)^\dagger F^T \tilde{J} F (Z^T I Z)^\dagger F^T. \end{aligned}$$

Next we check that

$$(Z^T I Z) = F^T (\tilde{I} + \tilde{C}) F.$$

By (16), we know

$$\left(\text{vec}^T(U^T \tilde{G}) \quad \text{vec}^T(\tilde{G}V) \right) = \text{vec}^T(\tilde{G})F = \text{vec}^T(\tilde{G}) \frac{\partial \text{vec}(A)}{\partial p^T} Z = 0.$$

So

$$\overline{UU}^T \tilde{G} = (\mathbb{I}_S - UU^T) \tilde{G} = \tilde{G} = \tilde{G}(\mathbb{I}_S - VV^T) = \tilde{G}\overline{VV}^T.$$

$$\begin{aligned} & Z^T I Z - F^T \tilde{I} F \\ &= Z^T \begin{pmatrix} 0 & 0 & 0 \\ 0 & 0 & \Lambda^{-1} \otimes \overline{V}^T \tilde{G}^T \overline{U} \\ 0 & \Lambda^{-1} \otimes \overline{U}^T \tilde{G} \overline{V} & 0 \end{pmatrix} Z \\ &= \begin{pmatrix} V^T \otimes \mathbb{I}_R & \mathbb{I}_R \otimes U^T \\ \overline{V}^T \otimes \mathbb{I}_R & \mathbb{I}_R \otimes \overline{U}^T \end{pmatrix}^T \begin{pmatrix} 0 & 0 & 0 \\ 0 & 0 & Q_{S-R,R}(\Lambda^{-1} \otimes \overline{V}^T \tilde{G}^T \overline{U}) \\ 0 & (\Lambda^{-1} \otimes \overline{U}^T \tilde{G} \overline{V}) Q_{R,S-R} & 0 \end{pmatrix} \begin{pmatrix} V^T \otimes \mathbb{I}_R & \mathbb{I}_R \otimes U^T \\ \overline{V}^T \otimes \mathbb{I}_R & \mathbb{I}_R \otimes \overline{U}^T \end{pmatrix} \\ &= \begin{pmatrix} 0 & ((\mathbb{I}_R \otimes \overline{U})(\Lambda^{-1} \otimes \overline{U}^T \tilde{G} \overline{V}) Q_{R,S-R} (\overline{V}^T \otimes \mathbb{I}_R))^T \\ (\mathbb{I}_R \otimes \overline{U})(\Lambda^{-1} \otimes \overline{U}^T \tilde{G} \overline{V}) Q_{R,S-R} (\overline{V}^T \otimes \mathbb{I}_R) & 0 \end{pmatrix} \\ &= \begin{pmatrix} 0 & ((\mathbb{I}_R \Lambda^{-1} \mathbb{I}_R \otimes \overline{UU}^T \tilde{G} \overline{VV}^T) Q_{R,S})^T \\ (\mathbb{I}_R \Lambda^{-1} \mathbb{I}_R \otimes \overline{UU}^T \tilde{G} \overline{VV}^T) Q_{R,S} & 0 \end{pmatrix} \\ &= \begin{pmatrix} 0 & ((\Lambda^{-1} \otimes \tilde{G}) Q_{R,S})^T \\ (\Lambda^{-1} \otimes \tilde{G}) Q_{R,S} & 0 \end{pmatrix}. \end{aligned}$$

$$\begin{aligned} F^T (V \Lambda^{-1} U^T \otimes \tilde{G}) Q_{S,S} F &= \begin{pmatrix} \mathbb{I}_S \otimes U^T \\ V^T \otimes \mathbb{I}_S \end{pmatrix} (V \Lambda^{-1} U^T \otimes \tilde{G}) Q_{S,S} (\mathbb{I}_S \otimes U \quad V \otimes \mathbb{I}_S) \\ &= \begin{pmatrix} V \Lambda^{-1} U^T \otimes 0 \\ \Lambda^{-1} U^T \otimes \tilde{G} \end{pmatrix} Q_{S,S} (\mathbb{I}_S \otimes U \quad V \otimes \mathbb{I}_S) \\ &= \begin{pmatrix} 0 \\ Q_{R,S} \tilde{G} \otimes \Lambda^{-1} U^T \end{pmatrix} (\mathbb{I}_S \otimes U \quad V \otimes \mathbb{I}_S) \\ &= \begin{pmatrix} 0 & 0 \\ Q_{R,S} (\tilde{G} \otimes \Lambda^{-1}) & 0 \end{pmatrix} \\ &= \begin{pmatrix} 0 & 0 \\ (\Lambda^{-1} \otimes \tilde{G}) Q_{R,S} & 0 \end{pmatrix}, \end{aligned}$$

$$F^T \tilde{C} F = \begin{pmatrix} 0 & 0 \\ (\Lambda^{-1} \otimes \tilde{G}) Q_{R,S} & 0 \end{pmatrix} + \begin{pmatrix} 0 & 0 \\ (\Lambda^{-1} \otimes \tilde{G}) Q_{R,S} & 0 \end{pmatrix}^T = Z^T I Z - F^T \tilde{I} F.$$

□